Carbonate cementing minerals in rhizoliths from Badain Jaran Desert: Implication for pedo-diagenesis and environment of dune soil

Qingfeng Sun, Kazem Zamanian, Arnaud Huguet, Guido L B Wiesenberg, Tianlei Zhao, Ziqiang Lei

Carbonate cementing minerals in rhizoliths from Badain Jaran Desert: implication for pedo-diagenesis and environment of dune soil

Qingfeng Sun[a,b,c*], Kazem Zamanian[d], Arnaud Huguet[e], Guido L.B. Wiesenberg[f] , Tianlei Zhao[g], Ziqiang Lei[a]

[a]Key Laboratory of Eco-function Polymer Materials of the Ministry of Education, Northwest Normal University, Lanzhou, Gansu, P.R. China
[b]State Key Laboratory of Palaeobiology and Stratigraphy, Nanjing Institute of Geology and Palaeontology, CAS, P.R. China
[c]Key Laboratory of Resource Environment and Sustainable Development of Oasis, Gansu Province, Northwest Normal University, Lanzhou, Gansu, P.R. China
[d]Institute of Soil Science, Leibniz University of Hannover, Herrenhäuser Str. 2, 30419 Hannover, Germany
[e]Sorbonne Université, CNRS, EPHE, PSL, UMR METIS, F-75005 Paris, France
[f]Department of Geography, University of Zurich, Zurich, Switzerland
[g]CAS Key Laboratory of Crust-Mantle Materials and Environments, School of Earth and Space Sciences, University of Science and Technology of China, Hefei, P.R. China.

Abstract

Pedogenic carbonates are a good proxy of soil formation and functioning because the morphology of minerals is directly related with the processes of dissolution–precipitation. Carbonate rhizolith is one type of pedogenetic carbonate forming in modern soils of dunes and loess. The calcite micro-morphology with the sedimentary hydrogeochemical conditions prevailing during their formation remains open. Electron microscopy with an X-ray energy dispersive spectrometer and X-ray diffraction were used to investigate in detail the micro-morphology of carbonate cements of the rhizoliths and obtain paleoenvironmental information in the dune soil of Badain Jaran Desert in Northwest China. Two types of carbonates rhizoliths, primary rhizoliths (PR) and reworked rhizoliths (RR), were found. The PRs are

present *in situ* within dune soils. The RRs are being eroded out from soil, potentially dislocated or transferred, and weathered at the soil surface. PRs displayed homogeneous micritic mass of calcite crystals, with pores, cavities and voids among the mass. RRs displayed various morphologies of calcite crystals (polyhedral, euhedral rhombic, tooth-like, prismatic and pillar), rosettes, short rods, and calcified fungal hyphae. The diagenesis differences at soil depth and surface affected the crystal morphologies. The homogeneous micritic mass of calcite crystals of the PRs were formed during the early diagenesis, preferentially in wet soils with semi-closed and semi-redox conditions. In contrast, the cementing minerals of the RRs became bigger and clearer in the late diagenesis than during early diagenesis due to recrystallization in open, dry and oxidative conditions at the soil surface. Therefore, the cement crystal morphologies of the rhizoliths can reflect the local environmental and climatic conditions. These objects can be used as environmental and pedo-diagenesis proxies in dune soil or sediments, recording the associated conditions of moisture, temperature, wind, erosion, weathering, solar radiation at the soil surface or at depth. Therefore, assessing the micromorphology of pedogenic carbonates has important implications for soil ecology and evolution as well as plant root physiology in deserts.

Keywords

Carbonate minerals; Scanning electron microscopy; Energy dispersive X-ray spectroscopy; X-ray diffraction; Crystal morphology; Soil diagenesis environment

1.Introduction

Calcium carbonate ($CaCO_3$) mostly exists in three crystalline forms, which are, in the order of stability, calcite, aragonite and vaterite (e.g., Gopi et al., 2013; Sekkal & Zaoui, 2013; Addadi & Weine.,1997; Simkiss, 1964). Vaterite crystals have a hexagonal structure, and aragonite crystals show an orthorhombic structure, while

calcite crystals present a rhombohedral structure (Liendo et al., 2022; Jimoh et al., 2018). Investigating the micro-morphology of calcium carbonate in soils, sediments and rocks can help in reconstructing past environmental conditions (Alonso-Zarza, 2018; Verrecchia & Verrecchia, 1994; Monger et al., 1991) The occurrence and morphology of pedogenic carbonates, including size, shape and distribution are valuable indices of pedo-environments and pedogenic processes (Golubtsov et al., 2021; Nyachoti et al., 2017; Durand et al., 2018; Diaz-Hernandez et al., 2018; Milliere et al., 2018; Eren et al., 2018).

Calcium carbonate found specially in rhizosphere microecosystems shows a unique relationship with several factors such as organic matter, micro-organism and plant distribution, as well as moisture and leaching processes (Huguet et al., 2020; Casado et al., 2014; Becze-Deák et al., 1997). Carbonate micro-morphology includes calcified root cells (*Microcodium*), $CaCO_3$ hypocoatings, needle fiber calcite, powdery calcite coatings, and calcite pseudomorphs on gypsum (Golubtsov et al., 2021; Kosir, 2004; Becze-Deák et al., 1997). However, despite many decades of thorough descriptive and interpretative work of these minerals, relating calcite micro-morphology with the predominant sedimentary hydrogeochemical conditions during their formation remains a challenge. Environmental interpretations of the calcite micro-morphology have been hampered by the fact that the calcite morphogenesis results from complex interactions between different physico-chemical parameters which often act simultaneously (e.g., carbonate mineral supersaturation, Mg/Ca ratio of the parental fluid, organic and inorganic additives, Mercedes-Martín et al., 2021).

The micro-morphology of calcium carbonate within carbonate rhizoliths, such as calcite rhomb chains, isolated calcite rhombs, calcified spherical bodies, calcified epilithic and chasmolithic filaments, grain-coating calcite needle mats, is related to their formation characteristics (Jones & Ng, 1988). Since the factors controlling the morphology of calcite crystals are not fully understood, it is necessary to rely on other materials to obtain an insight into this aspect of the problem. There is probably no

universal cementation scheme for rhizoliths, the characteristics of the cements being a function of the local conditions. The nature of the plants themselves may play an extremely important role in the cementation of rhizosphere (Sun et al., 2021, 2020; Marasco et al., 2018) or within roots (Huguet et al., 2021; Luo et al., 2021; Gocke et al., 2014). Plants were shown to have an obvious effect on the diagenesis of carbonates in vadose environments (Sun et al., 2021, 2020; Marasco et al., 2018; Jones & Ng, 1988). Nevertheless, the characteristics of the cements can be controlled to a large extent by the activity of the microorganisms that are associated with the plant roots.

A large number of studies on rhizoliths has been published over the last decades, but detailed investigations of the microscopic morphology of calcium carbonate within carbonate rhizoliths remain scarce, with the description of microscopic morphology of calcium carbonate included in some case studies (e. g., Sun et al., 2021, 2020, 2019a, b,c; Gao et al., 2020a, b; Huguet et al., 2020; Li et al., 2020, 2017, 2015a, b; Zhu et al., 2019; Alonso-Zarza, 2018; Barta, 2011; Klappa, 1980). Nevertheless, pedogenic carbonates are a good promising proxy of soil formation and functioning because the morphology of minerals is directly related with the processes of dissolution–precipitation. Thus, they can provide information on climate and water regime dynamics during or even after the lifetime of plants, whose roots entail formation of these structures. Electron microscopy with an X-ray energy dispersive spectrometer (SEM/EDS) was shown to be a powerful tool to investigate in detail the micro-morphology of carbonate cements and obtain paleoenvironmental information (Kuznetsova & Khokhlova, 2012).

Apart from many other known areas worldwide, carbonate rhizoliths of the Alashan Deserts of Northwest China have been intensively studied over the recent years using different tools (lipid biomarkers, ^{14}C dating, major and trace elements, phytoliths, cementing mineral morphology, carbon and oxygen isotopes), allowing the historical analysis of climate change (Sun et al., 2021, 2020, 2019a, b; Li et al., 2020, 2017, 2015a, b; Gao et al., 2020a, b; Zhu et al., 2019). However, only few information

on rhizolith genesis were obtained. Several key issues remain open, such as the age and formation mechanisms of the rhizoliths, including the influence of the vegetation type and soil microbial diversity on the formation of these objects (Sun et al., 2021, 2020). For instance, the rhizolith ages remain often unclear due to the age discrepancies between their carbonate cementing minerals and the inner root relicts (Sun et al., 2019a). The influence of climate change on the root tubes (Li et al., 2015) has still to be investigated. This is even further complicated by the fact that the rhizoliths are often not found in intact relationship with their forming plants. The identification of traces of life based on rhizolith characterization is usually challenging, especially in very old rocks, as the morphological and chemical signatures of biominerals and microfossils are subtle, of microscopic size and inevitably altered with aging. Nevertheless, the rhizoliths of the Alashan Deserts are of special interest, as they were shown to form only around the dead roots of *Artemisia* and to save the complete information of mineralization of calcium carbonate during Holocene in modern dune soils through pedodiagenetic effects (Sun et al., 2021, 2020). Therefore, this work aimed at investigating the micro-morphology of calcium carbonate of the rhizoliths occurring in dune soils from Badain Jaran Desert in the Alashan Deserts. Such a study was performed using SEM, EDX and XRD. The cement micro-characteristics of the carbonate rhizolith were related to the environmental conditions and processes taking place in and on the soils, allowing to better constrain the conditions of these objects as environmental proxies. This study provides a reference and model for future rhizolith studies of deserts worldwide.

2. Study area

Badain Jaran Desert (BJD) (39°04′15″N to 42°12′23″N, 99°23′18″E to 104°34′02″E) is in North-western China (Fig. 1a, b), covering an area of approximately 52,100 km^2. It is subjected to a transitional climate between the Asian summer monsoon and westerly belt (Wang F., et al., 2015). The elevations of the BJD

range between 1,000 and 1,500 m a.s.l. and decrease from southeast to northwest (Zhu et al., 2010). This desert comprises the tallest mega-dunes the world, generally 200–300 m high and 3-5 km long, with lakes frequently occurring between the dunes. The latter are especially dense in the south-eastern portion, where they can reach up to 500 m a.s.l. Towards the northwest alluvial/lacustrine plain, the size of sand dunes progressively decreases and the lakes gradually disappear (Fig. 1, 2).

The mean annual precipitation is currently 40–120 mm, falling mainly in summer. The mean annual potential evaporation is over 2500 mm. The conventional precipitation (below 5 mm) accounts for approximately 90% of rainfall events (Wang et al., 2013). The soil heat flux shows the largest diurnal variations at 5 cm depth and only slight variation at 20 cm depth (Li et al., 2012). The mean annual air temperature ranges from 9.8 to 10.2°C and the mean annual wind speed varies from 2.8 to 4.6 m/s. The prevailing wind direction over the year is northwest, related to the winter monsoon from the Siberian High-Pressure System (Zhang et al., 2017).

The vegetation of this desert is dominated by shrubs and subshrubs, including *Artemisia, Agriophyllum, Triglochin, Glaux, Aeluropus, Haloxylon, Nitraria, Tamarix,* and *Reaumuria* species (Wang M. et al., 2015; Yang et al., 2003).

The dune soil sand sources are the weathered debris and sediments of the northwest Gobi and the alluvial fan of the Heihe river. The northwest winds and windstorms have transported them to the desert (Fig. 1. Dong et al., 2013, 2009). The grain size of surface sand is dominated by well-sorted, rounded, pinky-grey, middle to fine sand (of feldspar and quartz), containing only slight amount of melanocratic minerals (such as hornblende, pyroxene and magnetite). Carbonate minerals are in low abundance in the silicate desert sands (Bai, 2011; Gates et al., 2008). The average carbonate content in soils was reported as 4.6 % by Wang et al. (2004) and 6.5 % by Sun et al. (2019a).

The thickness of the upper dry layer of the mega-dunes in this desert is only about 20-30 cm, with a conspicuous wet layer under the upper dry layer. Between 0.2-1.5 m depth, the water content is usually 1-5% (wt, Wang et al., 2019; Zhao et al.,

2011; Gu et al., 2004) and is up to 10% at 90 cm depth with well-preserved sand bedding (Liu et al., 2016). At 2 m depth, water content is about 65% (pore saturation; Zhao et al., 2011). Water in the sandy soil layer is mainly divided into adsorbed water and gravity water. Adsorbed water exists in the form of a water film and is thus termed film water. It is generally thought that if the water content of the sand layer is <3% then it is adsorbed water, and if the water content is >3% then it is gravity water. Adsorbed water, which is derived from rainfall, moves slowly downwards and is generally a minor contribution to groundwater (Zhao et al., 2017). In contrast, gravity water moves rapidly downwards within a soil and is the most important supplement of groundwater in depressions and lakes. Gravity water with a content above 5% (wt) was found in some sand layers of the BJD (Zhao et al., 2017). The precipitation in this desert plays an important role by providing water to the soils and lakes (Ma et al., 2019; Yue et al., 2019). However, in somewhere in the hinterland of the desert, the soil water contents are uneven and variable from 0.36-2.98% along depth changes from 4.3-9.7m, due to micro-geomorphologies differences (Dong et al., 2022; Zhao et al., 2017). Soil water content is less in the surface soil because it suffers stronger evaporation, while the deep soil water (> 200 cm) is hardly influenced by the evaporation (Jin et al., 2021).

3. Methods

Because of the vast sand sea area, poor accessibility and the dominance of an extremely arid climate, field explorations were only conducted in zones located in the south-eastern part of the desert, where many mega-dunes, lakes and low small dunes next to the desert margin are present (Fig. 1, 2). In the exploration area in the hinterland of the desert, rhizoliths were only found at six sites (Fig. 2, red points A-F). Detailed survey and examinations for landscape, vegetation, modern root, sediment/soil, rhizolith exposure and morphology were carried out around these sites. At each site the most representative samples of carbonate rhizoliths and their typical

features were intensively described and photographed. Typical rhizolith samples were collected for laboratory analyses and further photographing (Sun et al., 2021).

Care was taken to keep the rhizoliths intact for detailed description of their characteristics in the field down to the ultramicroscopic observations in the laboratory. Samples were chosen based on their typical external characteristics for determining scanning electronic microscopy. Energy dispersive X-ray spectroscopy, micro-morphological texture and cement mineralogy analyses by microscopy, as well as cathodoluminescence and staining were all performed at the Institute of Northwest Petroleum Geology, Lanzhou, China (Sun et al., 2021). The micro-scale morphology and chemical compositions of the rhizolith cement were determined by scanning electronic microscopy (SEM; FEI Quanta 450) coupled with Energy dispersive X-ray spectroscopy (EDS). Fragments of the rhizoliths were gold coated, and then analysed by SEM coupled with EDX, as previously described (Sun et al., 2021). Powder X-ray diffraction (XRD) was recorded on a Japan Rigaku Smart Lab X-ray diffractometer using Cu-Kα irradiation (λ= 0.154056 nm) to determine the mineral phase, and the sample was scanned from 10 to 70º 2θ and at a step of 0.02º, at CAS Key Laboratory of Crust-Mantle Materials and Environments, School of Earth and Space Sciences, University of Science and Technology of China, Hefei, China. The micro-morphological terms of carbonate minerals crystals are employed based on Mercedes-Martín et al. (2021) and Minerals.net (https://www.minerals.net/mineral/calcite.aspx).

4. Results

4.1. Field features of rhizoliths

Two types of rhizoliths were distinguished based on the outcrop states: reworked (RR) and primary rhizoliths (PR). The RRs are being eroded out from soil, potentially translocated and weathered on the soil surface under solar radiation and wind erosion, and they are thinner and harder than the PRs. In contrast, the PRs are present within

231 dune soils and keep their original characteristics *in situ*, without being eroded,
232 transferred and weathered.

233 **4.1.1 RRs on soil surface**

234 RRs were only found in Sites A, B and C. Their general features are described
235 below.

236 At site A (Sumujilin Lake, 39°48'N, 102°26'E), the rhizolith outcrops were
237 found at the feet of the windward gentle slopes of the mega-dunes situated above the
238 east of the Sumujilin Lake (Fig. 3a). Brown purple RRs were present as fragments
239 eroded out of the sand. The fragments of typical rhizoliths with bright dark brown
240 colour and rills are hard and varnished brightly. Their centres are hollow (Fig. 3b).

241 At Site B (Nuoertu Lake, 39°46'N, 102°27'E), rhizolith outcrops were found
242 along the gentle slopes of the mega-dunes on the east side of the Nuoertu Lake. RRs
243 occurred as enormous fragments as at Site A. However, the fragments were white,
244 corresponding to the inner parts of the central hollows of former roots subjected to
245 weathering. In some rhizoliths, relicts of fine root hairs were observed. Weathered
246 rills were apparent on the outer surfaces of the big tubes. The small broken pieces of
247 rhizoliths were white and fragile due to weathering (Fig. 4).

248 At Site C (Baoritaolegai Lakes, 39°35'N, 102°28'E), rhizoliths were also
249 found along a windward gentle slope between two mega-dunes, south of Baoritaolegai
250 Lakes. RRs were found as broken tubes. Their general features are similar to the
251 above sites (photos were omitted).

252 **4.1.2 Vertical RRs above soil and PR features within soil**

253 Both PR and RR were found at Sites D, E, F. But the RRs are vertical above
254 soil and they are the upper parts of the PR underground.

255 At Site D (6.0 km east to the Gate of the BJD National Geological Park,
256 39°27'N, 102°26'E), RRs fragments are lying intricately at the sand surface. However,
257 only a few of the RRs were found standing vertically above soil. PRs are present
258 underground, below the vertical standing rhizoliths above soil surface. The upper part
259 above ground is thinner and harder than the underground primary part within soil

because of weathering and erosion (Fig. 5a). Once broken, they display decayed root relicts within the central hollowness, surrounded by a white hale carbonate cement (Fig. 5b). After having been dug out for some time, they became harder quickly than before due to losing soil water at the site.

At Site E (39°25′14.56″N,102°8′55.25″E), their general features are similar to those of Site D. After having been dug out, the PR show brown interior with preserved root relicts when broken (Fig. 6). PR are soft, while RR are hard.

At Site F (39°29′57″N,102°12′48″E), their general features are similar to those of Site D. PR were broken easily by gentle hand-force. The centre of the decayed root relicts is brown (photos were omitted).

4.2. SEM features and EDS mineral compositions of rhizolith cement

Ten rhizolith specimens – one or two from each site - were chosen for laboratory analyses, with determination of micro-morphological texture and mineral composition. Their SEM features differ from each other and are detailed below.

4.2.1 RRs on soil surface

Site A

The cement of the RR is tight and densely compact around the sand particles (Fig. 7a). Some of the cementing minerals show polyhedral crystals and many pores occur within the cement (Fig. 7b). They also display bigger euhedral rhombic crystals, or tooth-like crystals around the walls of the pores, against the dense fine crystal cement background (Fig. 7c). Moreover, they present both aragonite rosette morphology (Fig. 7d) and equant polyhedral crystals characterized by well-developed crystal faces and slightly smooth edges and corners (Fig. 7e). Generally, all EDS spectra reveal that the cements are calcium carbonate (Fig. 7f).

Site B

The cement of the RR is compactly tight and dense around sand particles (Fig 8a). The morphology of the cementing minerals shows polyhedral (Fig. 8b) and short

rods crystals (Fig. 8c). Their mineral compositions are calcite with a little of Mg (Fig. 8d) based on EDS analysis.

Site C

The cement of the RR is not as tight and densely compacted around sand particles as it was at sites A and B. However, the cement shows short rods shape (Fig. 9a) and calcified fungal hyphae-like networks with many pores, cavities and voids (Fig. 9b). The cement is calcium carbonate, as indicated by EDS (spectrum is omitted).

4.2.2 Vertical RRs and PRs

Site D

The rhizoliths are constituted of two parts, the upper parts-RR at the soil surface and the lower parts-PR within soil. The RR cement shows short rods crystals (photo is omitted). The PR either displays homogeneous micritic mass (Fig. 10a) with a lot of pores, cavities and voids (Fig. 10b), or dense prism/pillar-like calcite crystals (Fig. 10c). The cement is mainly constituted of calcium carbonate with only low amounts of Mg (EDS spectrum is omitted).

Site E

At this site only one PR was analysed. The lab tests of upper RRs were done. The cementing minerals are homogeneous micritic mass, which are growing along the surfaces of sand particles (Fig. 11a). The calcite crystals form thinner layers without obvious and clear crystal shapes and not thick enough to fill the pores among the particles (Fig. 11b, c). Based on EDS analysis, the cement composition is calcium carbonate. (Fig. 11d).

Site F

Similar to site D, the cement of the RRs above soil surface is made of short rods crystals (photo is omitted). The PR within soil display homogeneous micritic mass (Fig. 12), with pores, cavities and voids (photo is omitted). The PR cement is mainly

constituted of calcium carbonate with low amounts of Mg and NaCl (EDS spectrum is omitted).

The micro-morphologies and compositions of the cementing minerals and their diagenesis features are summarised in the Fig. 13. The micro-morphologies show the following key features: (i) the PRs have homogeneous micritic mass, with pores, cavities and voids; (ii) the RRs on or above soil surface have big and clear (polyhedral, euhedral, rhombic, prismatic, rosette) crystal shapes and short rods, with occasional hair-like, or fungi-form crystals; (iii) vertical upper RRs of the PR have only short rods; (iv) the cement minerals compositions is calcium carbonate with a little of Mg.

4.3. XRD mineral compositions of rhizolith cement

XRD results confirmed that the carbonate cements are all calcite (Fig. 14). In addition, sand particles like quartz and plagioclase feldspars (matched well with standard card of anorthite and anorthite, sodium) were also detected. This is consistent with section cathodoluminescence observations (Sun et al., 2021).

At sites A, C and F, SEM showed that aragonite is also present by its shape in the cement. However, no diffraction peaks of aragonite were detected in the corresponding XRD results. Therefore, the content of aragonite is likely too low to be detected by XRD (Fig. 14a, c, f).

5. Discussion

5.1 General SEM characteristics of the cement of the PRs and biogeochemical implications

5.1.1 Early diagenesis features within soil

Within the underground dune soil, the diagenesis environment of primary rhizoliths is characterized by weak redox conditions (due to semi-closed conditions) with comparatively higher moisture content, and lower stable temperature than those

at the soil surface. Therefore, the conditions of the early diagenesis process are comparatively steady in deep soils.

Within soil, vascular plants and symbionts increase chemical weathering of the silicates, which results in increasing of Ca^{2+} and HCO_3^- availability and pedogenetic carbonate production (Brasier, 2011). There are two Ca^{2+} sources for rhizolith cement: 1) authigenic carbonates from in situ chemical weathering of soil primary silicate minerals such as feldspar, mica, amphibole and pyroxene; and 2) dissolution of in situ primary lithogenic carbonate rock debris such as limestone and dolomite (Sun et al., 2019a). Moreover, dead root decomposition leads to increased CO_2 and HCO_3^- production around the rhizosphere (Sun et al., 2021,2020). Then dry periods increase the calcium concentration in the soil solution from which $CaCO_3$ precipitates by the evapotranspiration and release of CO_2 with temperature rise (Sun et al., 2022, 2021,2020). Precipitation is also associated with the dissolution and recrystallization of carbonate taking place in the parent matrix, such as soil, sediment and rocks (Eren et al., 2008). In the dune soil of this desert, the semi-closed environment is favourable to both root organic decay and formation of HCO_3^- solutions among the pores of the sandy soil. However, the balance between root decay-CO_2-HCO_3^- and calcite growth is the key point making the soil micro-environment around the dead roots favourable to the aforementioned process. Such a balance is controlled by factors like soil moisture, soil depth, wind, as well as precipitation or/and temperatures. Such parameters could not be measured in the field but would have been useful to better understand the details of rhizolith diagenesis.

5.1.2 Origin and implications of cement crystal micro-morphology

Under the aforementioned diagenesis conditions, the cementing minerals of the primary rhizoliths display (i) homogeneous micritic mass in thin layers without obvious and clear crystal shapes, precipitating mainly on particles surface (Fig. 10a; 11a, b, c;12); (ii) prism/pillar-like calcite (Fig. 10c); and occasionally (iii) pores,

cavities and voids among the micritic mass (Fig. 10b). Their origins and implications are explained as follows.

The presence of homogeneous micritic mass implies that the fine calcite crystals were in their initial nucleation and quickly precipitated at the beginning of diagenesis, which cannot be observed even under high magnification (Zhou & Chafetz, 2009; Alonso et al., 2004).

The prismatic/pillar-like calcite crystals were subjected to diagenesis for a longer time than homogeneous micritic mass, as shown by the larger size of the former. This suggests that the supersaturation degree of mineral solution changed during the mineralization. During the formation and precipitation of crystals, the solution became supersaturated, allowing the formation of the crystal nucleus. Then, the diffusion and precipitation of ions at the surface of the crystal nucleus led to the crystal nucleus growth and later to the formation of crystal particles and even big crystals when concentrated. If the supersaturation degree is too high, the reaction of Ca^{2+} and CO_{2-3} will be too quick to control the crystal morphology. In contrast, when the supersaturation degree is low, the growth velocity of crystal is low, letting enough time to the formation of the surficial crystal (Cheng et al., 2014). An experiment investigating the precipitation of non-marine calcite confirmed that low calcite supersaturation conditions are prone to form single-crystal prismatic to di-pyramid calcite precipitates (Mercedes-Martin et al., 2021). This suggests that homogeneous micritic mass cement formed rapidly, with enough CO_2 supplied by root decay, and that the short rods calcite crystals formed in low concentration of mineral solutions and/or were subjected to secondary diagenesis after having been formed.

The pores, cavities and voids in calcite cement imply that microorganisms and CO_2 gas played key roles in calcium carbonate crystallization through fermentation effect. This is supported by the following evidences from previous studies: (i) These characteristics are similar to those of the carbonate crystals in Mu Us Desert in northern China, with a rough and porous appearance caused by bacterial strains (Liu et al., 2018). Therefore, the pores, cavities and voids in the BJD rhizoliths might be

caused by microorganisms. (ii) Irregular carbonate crystals with broken faces and holes on surfaces were suggested to be formed in humid conditions (Kuznetsova & Khokhlova, 2012), which could be the case in the BJD. (iii) Increasing contents in (alginic) acid were shown to contribute to the formation of curved and poorly faceted crystal morphology with higher sphericity (Mercedes-Martin et al., 2021). This means that the pores, cavities and voids of the BJD rhizoliths could have been formed in an acidic microenvironment of soil. The release of CO_2 from *Artemisia* root decay could have led to the formation of such an acidic environment with gas bubbles (Sun et al., 2020).

These hypotheses are in agreement with the diagenesis features within deep dune soil and with the presence of microorganisms like fungi in the pores among sand particles. In fact, roots and associated microorganisms play a very important role for the pedogenic carbonate formation, not only around living roots (Eren et al., 2018), but also around dead roots (Sun et al., 2021,2020). For instance, microbialites have been found in desert soils and tropical forest soils as well. *Myxococcus*, usually found in soils rich in organic matter and decaying material, can precipitate calcium carbonate independently of being metabolically active or killed, though different polymorphs of calcium carbonate can be formed (Zhu & Maria, 2016). Root decay under microbial decomposition induce gases bubbles in mineral solution and produce calcite with pores, cavities and voids through different metabolic pathways. Most microbial cells provide nucleation sites for carbonate formation, with appearance of microbial textures like cavities, voids, fibric and hair-like shape. Previous studies also confirmed that carbonate precipitation can be caused by soil microorganisms (Khormali et al., 2020; Menezes et al., 2019; Wang et al., 2016; Zamanian et al., 2016; Vepraskas, 2015).

However, there is still an ongoing debate questioning whether the organisms were alive during the calcification (Eren et al., 2018). Where carbon comes from and whether atmospheric CO_2 can be deposited via this biomineralization process remain unknown, representing an important gap in the knowledge of carbon sequestration via

426 microbial carbonate deposition (Liu et al., 2018). In this case, organisms may use root
427 remains as the source of carbon for biomass growth, resulting in increased
428 concentrations of calcium along the dead roots, with fungi digesting carbon
429 acquisition, leading to $CaCO_3$ precipitation. This process can take place both at the
430 surface or belowground. It is unclear whether microorganisms act like a catalyst by
431 increasing the medium pH, leading to the saturation of soil solutions and causing
432 calcite precipitation (Barta, 2011). Physicochemical and biogenic processes may have
433 worked together to form variant crystalline forms (Verrecchia & Verrecchia, 1994).
434 Overall, several factors should be further investigated in this desert: (i) the microbial
435 diversity in the bulk soil, both in living and dead rhizosphere; (ii) the microbial
436 influence on calcite formation; (iii) a better understanding of why rhizoliths are
437 formed only around the dead *Artemisia* roots.

438 5.2 General SEM characteristics of the cement of RRs and 439 biogeochemical implications

440 5.2.1. Late diagenesis features at soil surface

441 The Badain Jaren Desert is characterized by large thermal (day-night) amplitude
442 and seasonality, strong wind and little precipitation (cf 2. Study area). The
443 temperature at the desert surface soil can reach up to 70-80°C. Night temperatures in
444 deserts are typically much cooler than daytime temperatures (Khormali & Monger,
445 2020). This heat is transferred into the soil profile downward, with a gradient of about
446 0.5°C per 10 cm until the temperature reaches the approximate mean annual air
447 temperature at a depth of ca. 50 cm (Soil Survey Staff, 1999). Simultaneously, the
448 high-low temperature changes, extreme radiation and strong winds can enhance the
449 aridity of the surface soil, resulting in an increase of the mineral concentration in the
450 soil particle pores. Harsher conditions for microbial growth can be found in shallow
451 desert surface soils vs. deep ones, as only microorganisms resisting to high
452 temperatures can survive (Monger et al., 1991). The RRs are subjected to strong
453 aridity, high temperature changes, solar radiation, and furious wind at the dune

surface. Comparatively, the lying RRs on the soil surface are older than the vertical ones which are the upper parts of the PRs above ground.

5.2.2 Origin and implications of cement crystal micro-morphology

The cements of the RRs show the following characteristics: (i) the horizontal lying RRs: polyhedral crystals of calcite with well-developed crystal faces and slightly smooth edges and corners (Fig. 7b, e; 8a, b), or prismatic crystals (Fig. 7c; 8c), rosette shapes (Fig. 7d), calcified fungal hyphae networks (hair-like, or fungi-form crystals (Fig. 9b); (ii) the vertical RRs: short rods of aragonite (Fig. 9a). This implies the following regarding the origin and diagenesis conditions of the RRs:

As shown in Fig. 13, homogeneous micritic mass recrystallized to short rods and the short rods recrystallized to big clear (polyhedral, euhedral, rhombic, prismatic, rosette) crystals. Because the vertical RRs were eroded out from PRs present in soil, the formation of these short rods calcite crystals at the dune soil surface was subjected to a different diagenesis from the homogeneous micritic mass of PRs present underground. Recrystallization of homogeneous micritic mass of RRs took place after erosion and weathering due to the loss of soil water and the high temperature near the soil surface. Carbonate accumulations were formed in dry periods and in quiet conditions from solutions of normal concentration (Kuznetsova & Khokhlova, 2012). This is in line with a quick alternation of day-night temperatures (with fog some time) and short shower events in the desert, providing water for dune soil in depth and causing chemical weathering of soil minerals like feldspars and root decaying. Carbonate mineral solution forms in the soil. Then, strong alternating wet and dry conditions (due to strong wind, solar radiation and high temperature) promote and enhance the dissolution and precipitation of $CaCO_3$ and consequently formation of secondary carbonates (Becze-Deák et al., 1997; Borchardt & Lienkaemper, 1999). The diagenesis conditions at the soil surface support these micromorphological features of calcite cement. It was also confirmed by lab experiments, which showed that higher calcite supersaturation conditions tend to produce polycrystalline calcite

grains and corresponding aggregates (Mercedes-Martin et al., 2021). The polycrystalline calcite mentioned above should have been formed in high calcite supersaturation conditions, which were caused by high solar radiation, temperature and aridity around the surface soil.

Short rods and rosette shapes means aragonite occurrence in the cement. Aragonite crystals usually show rods (Ma & Feng, 2015; Boyjoo et al., 2014; Cheng et al., 2014; Sarkar & Mahapatra, 2012; Knez et al. 2006). Aragonite is more soluble (K_{sp}=6.3 * 10^{-9}) than calcite (K_{sp}=4.0 * 10^{-9}) at ordinary pressures and temperatures (25°C), and will commonly precipitate first from solutions. Aragonite is rare compared to calcite because it is thermally unstable and will transform to calcite. This process is more rapid in hydrous environments and at higher temperatures. For example, aragonite generally develops only under hot (e.g., springs) temperature conditions (Zeng et al., 2018; Balthasar & Cusack, 2015; Gutjahr et al, 1996). At ordinary temperatures the transition only takes place by dissolution of aragonite and precipitation of calcite (e.g., Chen et al., 2003; Degens, 1965). Moreover, aragonite is preferentially synthesized over calcite in the presence of (molten lauric) acid as an additive (Sarkar & Mahapatra, 2012). This implies that presence of an organic acid is favourable for aragonite formation. Acid solution formation needs acid gases like CO_2, H_2S, NO_2, etc. from decomposition of organic matter in aqueous soil. The decaying *Artemisia* roots satisfy the acid environment formation in the desert soil (Sun et al., 2021, 2020). The rosette shape particles which were observed result from the aggregation of aragonite rods. These characteristics were supported by the diagenesis features around the shallow soil of this desert. Hence, high temperatures, root decomposition and possible high local Mg/Ca from weathering of soil particles in shallow soil favour aragonite formation.

The fact that calcified fungal hyphae networks were found in cement (Fig. 9b) in the shallow soil or above the soil implies that soil microorganisms play a fundamental role in the genesis of calcic soils around the rhizosphere. Biomineralization of calcite by soil microorganisms has important implications for identifying subaerially exposed

sediments in the geological column (Wright, 1986). Calcified soil microorganisms, in addition, may serve as useful microfossils that reflect paleoclimatic conditions. The mechanism explaining the production of calcite by microorganisms is probably related to the exudation of excess Ca^{2+} by microorganisms, which concentrate Ca^{2+} on their external surfaces (Phillips et al., 1987). In addition, the production of CO_2 by microbial respiration contributes to the formation of bicarbonate ions (Arnott & Pautard, 1970), which prompts calcite precipitation. Organic matter decomposition is increased by warm temperatures but is decreased by dryness. Overall, such a decomposition is increased when the soil profile receives infrequent precipitation that activates the dormant microbial population. High decomposition rates combined with low carbon inputs explain the low amount of organic carbon in hot deserts (Khormali & Monger, 2020). Calcified hair-like filaments are widely accepted to be of fungal (hyphae) origin, but other micro-organisms such as algae, cyanobacteria, actinomycetes, and eubacteria, and root hairs may also form these filaments (Eren et al., 2018; Durand et al., 2010; Alonso-Zarza et al., 1998). The present results indicate that calcified fungal filaments (Monger et al., 1991) can also be formed in desert soils that were initially noncalcareous, and whose calcite can be attributed to pedogenesis.

The relationships between diagenesis environment and micro-morphologies of cementing minerals are summarized in Fig. 13. PRs are in the first step of diagenesis; the vertical upper RRs above ground of the PRs are in the second step of diagenesis; the RRs lying on soil surface are in the last step of diagenesis. The micro-morphologies of cementing minerals of PRs and RRs show different characteristics related to the different diagenesis environments: (i) homogeneous micritic carbonate mass with pores, cavities and voids formed at first diagenesis stage underground; (ii) short rods of aragonite formed at late diagenesis stage with higher temperature; (iii) big and clear carbonate mineral crystals formed at last diagenesis stage. Microorganisms are involved in the formation of calcified fungal hyphae networks in favourable conditions at the dune soil surface, as confirmed by the

presence of desert biological soil crust (e.g., Zhang et al., 2021; Qi et al., 2021; Zhao et al., 2020).

6. Conclusions

The characteristics of the cementing minerals of the carbonate rhizoliths in the Badain Jaran Desert are affected by (micro)environmental conditions in the dune sandy soil. These objects enable the assessment of past environmental conditions that prevailed during their formation.

Diagenesis environments are different between the deep and surficial dune soils in the desert. Within the deep soil, the moisture content is higher than at the surface and the temperatures are stable. In contrast, the soil surface is characterized by large day-night temperature amplitude coupled with strong wind deflation, erosion and weathering under solar radiation. Thereafter, primary and reworked rhizoliths are formed within and on the soil, respectively. The primary rhizoliths buried underground, the vertical reworked rhizoliths above soil, and the lying or horizontal root tubes on soil surface correspond to early, middle and late diagenesis steps. The calcium carbonate cement of the PRs buried underground mainly displayed homogeneous micritic mass calcite with pores, cavities and voids. In contrast, the upper vertical parts-RRs of the PRs show short rods-like calcite crystals. However, the lying or horizontal RRs displayed a large variety of morphology (polyhedral crystals of calcite with well-developed crystal faces and slightly smooth edges and corners, or euhedral rhombic crystals, or prismatic/tooth-like crystals; rosette shapes and short rods of aragonite; prismatic/pillar crystals; calcified fungal hyphae). This confirms that the mineral crystalline morphologies are deeply affected by the different diagenesis stages and are dependent on the nature of the soil environments. Homogeneous micritic calcite crystals are formed during the initial stages of diagenesis underground with a stable environment with wet soil, semi-closed and -redox conditions. In contrast, the presence of polyhedral crystals of calcite with well-developed crystal faces and slightly smooth edges and corners, or euhedral

rhombic crystals, or prismatic/tooth-like crystals as well as rosette shapes and short rods of aragonite imply recrystallization through secondary diagenesis with complex and long processes at the soil surface. Aragonite is preferentially formed at higher temperature and with higher concentration of mineral solution in shallow soil environments. The presence of calcified fungal hyphae networks (hair-like, or fungi-form) crystals and pores, cavities and voids somewhere among the micritic mass indicate the role of microorganisms in calcium carbonate crystallization. The extreme environmental conditions and lack of water at the soil surface in hyper-arid deserts hamper microbial life, allowing only highly specialized microbial communities to grow and survive, specifically at the soil surface.

The micro-morphological characteristics of the rhizolith cement shows that they can be good proxies for soil formation, evolutions, pedologic and diagenesis processes, especially around and within rhizosphere in desert soil. This study provides a good reference and model for the rhizolith study of deserts worldwide.

Declaration of competing interest

The authors declare that they have no known competing financial interests or personal relationships that could have appeared to influence the work reported in this paper.

Acknowledgements

We thank Prof. Gentao Zhou, Prof. Hong Wang and Dr. Zhen Liu for their suggestions. Funding for this work was supported by Sino-German Scientists Cooperation and Exchanges (M-0069, Sino-German Scientific Centre, National Natural Science Foundation of China) and State Key Laboratory of Palaeobiology and Stratigraphy (Nanjing Institute of Geology and Palaeontology, CAS. #223125).

References

596 Addadi L, Weiner S.,1997. Biomineralization: A pavement of pearl. Nature 389,
597 912-915.
598 Alonso-Zarza, A. M., 2018. Study of a modern calcrete forming in Guadalajara,
599 central Spain: an analogue for ancient root calcretes. Sedi. Geol. 373, 180-190.
600 Alonso-Zarza, A.M., Genise, J.F., Cabrera, M.C., Mangas, J., Martín-Pérez, A.,
601 Valdeolmillos, A., Dorado-Valiño, M., 2008. Megarhizoliths in Pleistocene
602 aeolian deposits from Gran Canaria (Spain): ichnological and
603 palaeoenvironmental significance. Palaeogeo. Palaeoclim. Palaeoecol. 265,
604 39-51.
605 Alonso-Zarza, A.M., Silva, P.G., Goy, J.L., Zazo, C., 1998. Fan-surface dynamics and
606 biogenic calcrete development: interactions during ultimate phases of fan
607 evolution in the semiarid SE Spain (Murcia). Geomorph. 24, 147-167.
608 Arnott, H.J., and Pautard, F.G.E., 1970, Calcification in plants, in Schraer, H., ed.,
609 Biological calcification: Cellular and molecular aspects: New York,
610 Appleton-Century-Crofts, 375-441.
611 Bai, Y., 2011. Internal Structure and Formation Process of Mega-Dunes in the Badain
612 Jaran Desert (in Chinese with English abstract). Doctoral dissertation. Lanzhou
613 University.
614 Balthasar, U., Cusack, M., 2015. Aragonite-calcite seas–Quantifying the gray area.
615 Geol. 43:99–102.
616 Barta, G., 2011. Secondary carbonates in loess-paleosoil sequences: a general review.
617 Cent. Eur. J. Geosci 3 (2), 129-146.
618 Becze-Deák, J., Langohr, R., Verrecchia, E., 1997. Small scale secondary $CaCO_3$
619 accumulations in selected sections of the European loess belt: morphological
620 forms and potential for paleoenvironmental reconstruction. Geoderma 76,
621 221-252.
622 Borchardt, G., Lienkaemper, J.J., 1999. Pedogenic calcite as evidence for an early
623 Holocene dry period in the San Francisco Bay area. California. Geol. Soci. Amer.
624 Bull. 111 (6), 906-918.

625 Boyjoo, Y., Pareek, V. K., & Liu, J., 2014. Synthesis of micro and nano-sized
626 calcium carbonate particles and their applications. J. Mater. Chem. A 2(35),
627 14270.
628 Brasier, A.T., 2011. Searching for travertines, calcretes and speleothems in deep time:
629 Processes, appearances, predictions and the impact of plants. Earth Sci. Rev. 104,
630 213-239.
631 Casado, A. I., Alonso-Zarza, A. M., & Iglesia, A. L. 2014. Morphology and origin of
632 dolomite in paleosols and lacustrine sequences. examples from the Miocene of
633 the Madrid Basin. Sediment. Geol. 312, 50-62.
634 Cheng, H., Zhang, X., & Song, H., 2014. Morphological investigation of calcium
635 carbonate during ammonification-carbonization process of low concentration
636 calcium solution. J. Nanom. 1-7.
637 Chen, X. Y., Lintern, M. J., & Roach, I. C., 2002. Calcrete: Characteristics,
638 distribution and use in mineral exploration. CSIRO Exploration and Mining,
639 Kensington, Western Australia 6151, The University of Canberra, Division of
640 Science and Design, Australian Capital Territory 2601.
641 Diaz-Hernandez, J., L., Sanchez-Navas, A., & Delgado, et al., 2018. Textural and
642 isotopic evidence for ca-mg carbonate pedogenesis. Geochimica et
643 Cosmochimica Acta: Journal of the Geochemical Society and the Meteoritical
644 Society, 222, 485-507.
645 Dong, P, Liang, A., and Zhou, Y., 2022. Advancement of megadunes and its
646 implications in the Badain Jaran Sand Sea. Front. Earth Sci. 9:811181.
647 Dong, Z.B., Qian, G.Q., Lv, P., Hu, G.Y., 2013. Investigation of the sand sea with the
648 tallest dunes on Earth: China's Badain Jaran Sand Sea. Earth Sci. Rev. 120, 20 –
649 39.
650 Dong, Z., Qian, G., Luo, W., Zhang, Z., Xiao, S., Zhao, A., 2009. Geomorphological
651 hierarchies for complex mega-dunes and their implications for mega-dune
652 evolution in the Badain Jaran Desert. Geomorph. 106 (3), 180-185.

653 Degens, E.T. 1965. Geochemistry of sediments, a brief survey. Prentice-Hall, Inc.
654 Englewood Cliffs, New Jersey. 342pp.
655 Durand, N., Monger, H.C., Canti, M.G., Verrecchia, E.P., 2018. Calcium carbonate
656 features-chapter 9. In: Stoops, G., Mees, F., Marcelino, V. (Eds.), Interpretation
657 of Micromorphological Features of Soils and Regoliths, 2nd ed. Elsevier,
658 205-258.
659 Eren, M., Kadir, S., Hatipoğlu, Z., Gül, M., 2008. Quaternary calcrete development in
660 the Mersin area, southern Turkey. Turk. J. Earth Sci. 17, 763-784.
661 Eren, M., Kaplan, M. Y., Kadir, S., Kapur, S., 2018. Biogenic (β-fabric) features in
662 the hard laminated crusts of the Mersin and Adana regions, southern Turkey and
663 the role of soil organisms in the formation of the calcrete profiles. Catena
664 168,34-46.
665 Gates, J., Edmunds, M., Darling, G., Ma, J., Pang, Z., Young, A., 2008. Conceptual
666 model of recharge to southeastern Badain Jaran Desert groundwater and lakes
667 from environmental tracers. App. Geoch. 23, 3519-3534.
668 Gao, Y., Li, Z., Zhu, R., Wang, N., 2020a. Quantitative reconstruction of Holocene
669 millennial‐scale precipitation in the Asian monsoon margin of northwest China,
670 revealed by phytolith assemblages from calcareous root tubes in the Tengger
671 Desert. Cli. Dyn. 55,755-770.
672 Gao,Y., Li, Z., Zhu, R., Liao, H., 2020b. Stable isotope compositions, sources and
673 paleoenvironmental significance of Holocene calcareous root tubes in the
674 Tengger Desert, Northwest China. Catena 195, 104846.
675 Gocke, M., Peth, S., Wiesenberg, G.L.B., 2014. Lateral and depth variation of loess
676 organic matter overprint related to rhizoliths – revealed by lipid molecular
677 proxies and X-ray tomography. Catena 112, 72-85.
678 Gopi, S., Subramanian, V. K., & Palanisamy, K., 2013. Aragonite–calcite–vaterite: a
679 temperature influenced sequential polymorphic transformation of $CaCO_3$ in the
680 presence of DTPA. Mater. Res. Bull. 48(5), 1906-1912.

681 Gu, W.Z., Chen, J.S., Wang, J.Y., Zhao, X., Xie, M., Lu, J., Seiler, K. P., 2004.
682 Challenge from the appearance of vadose water within the surface layer of
683 megadunes, Badain Jaran dune desert, inner Mongolia. Ad. Water Sci. 15(6),
684 695–699 (in Chinese with English abstract).
685 Gutjahr, A., Dabringhaus, H., Lacmann, R., 1996. Studies of the growth and
686 dissolution
687 kinetics of the $CaCO_3$ polymorphs calcite and aragonite. I. Growth and
688 dissolution
689 rates in water. J. Cryst. Growth 158, 296–309.
690 Huguet, A., Bernard, S., Khatib, R., E., Gocke, M., I., Wiesenberg, G., L. B., Derenne,
691 S., 2021. Multiple stages of plant root calcification deciphered by chemical and
692 micromorphological analyses. Geobio. 19(1), 75-86.
693 Jimoh, O. A, Ariffin, K. S., Hussin, H. B, & Temitope, A. E., 2018. Synthesis of
694 precipitated calcium carbonate: a review. Carbonates & Evaporites. Carb. Evap.
695 33,331–346.
696 Jin, K., Rao, W., Wang, S., et al.,2021. Stable isotopes ($\delta^{18}O$ and $\delta^{2}H$) and chemical
697 characteristics of soil solution in the unsaturated zone of an arid desert. J.
698 Radioanal Nucl Chem 330, 367–380.
699 Jones, B. and Ng, K.-C., 1988. The structure and diagenesis of rhizoliths from
700 Cayman Brac, British West Indies. J. Sediment. Petrol. 58, 457-467.
701 Khormali, F., Shahriari, A., Ghafarpour, A., Kehl, M., & Frechen, M., 2020.
702 Pedogenic carbonates archive modern and past precipitation change – a transect
703 study from soils and loess-paleosol sequences from northern Iran. Quat. Int. 552,
704 79-90.
705 Khormali, F., & Monger, C., 2020. Hot desert soils—global distribution and unique
706 characteristics. Geoderma Reg. 23, e00330,1-12.
707 Knez, S., Klinar, D., Golob, J., 2006. Stabilization of PCC dispersions prepared
708 directly in the mother-liquid after synthesis through the carbonation of (hydrated)
709 lime. Chem. Eng. Sci. 61(17), 5867-5880.

710 Kosir, A., 2004. Microcodium revisited: root calcification products of terrestrial
711 plants on carbonate-rich substrates. J. Sed. Res. 74, 845–857.
712 Kuznetsova, A. M., & Khokhlova, O. S., 2012. Submicromorphology of pedogenic
713 carbonate accumulations as a proxy of modern and paleoenvironmental
714 conditions. B. Soc. Geol. Mex. 64(2), 199-205.
715 Li, J. G, Ao, Y. H., Li, Z. G., 2012. Comparative analysis of radiation and energy
716 budget over Badain Jaran Desert on clear and cloudy days in summer. Prog.
717 Geog. 31(11), 1443-1451.
718 Li, Z., Wang, N., Cheng, H., Ning, K., Zhao, L., & Li, R., 2015a. Formation and
719 environmental significance of late Quaternary calcareous root tubes in the deserts
720 of the Alashan Plateau, northwest China. Quat. Int. 167-174.
721 Li, Z., Wang, N., Li, R., Ning, K., Cheng, H., & Zhao, L., 2015b. Indication of
722 millennial-scale moisture changes by the temporal distribution of Holocene
723 calcareous root tubes in the deserts of the Alashan Plateau, Northwest China.
724 Palaeogeo. Palaeoclim. Palaeoecol. 440, 496-505.
725 Li, Z., Gao, Y., & Han, L., 2017. Holocene vegetation signals in the Alashan Desert
726 of northwest China revealed by lipid molecular proxies from calcareous root
727 tubes. Quat. Res. 88(1), 60-70.
728 Li, Z., Zhu, R., Gao, Y., Chim, C., H., Liao, H., 2020. Recrystallization of Holocene
729 calcareous root tubes in the Tengger Desert, Northwest China and its effects on
730 the reliability of paleoenvironmental reconstruction results. Quat. Int. 562, 85-93.
731 Liendo, F., Arduino, M., Deorsola, F. A., & Bensaid, S., 2022. Factors controlling and
732 influencing polymorphism, morphology and size of calcium carbonate
733 synthesized through the carbonation route: A review. Powder Tech. 398,
734 117050:1-22.
735 Liu, S., Lai, Z., Wang, Y., Fan, X., Wang, L., Tian, M., Jang, Y., & Zhao, H., 2016.
736 Growing pattern of mega-dunes in the Badain Jaran Desert in China revealed by
737 luminescence ages. Quat. Int. 410, 111-118.

738 Liu, Z., Zhang, Y.Q., Fa, K. Y., Zhao, H.F., Qin, S.G., Yan, R., Wu, B., 2018. Desert
739 soil bacteria deposit atmospheric carbon dioxide in carbonate
740 precipitates. Catena 170, 64-72.
741 Luo, X., Wang, H., An, Z., Zhang, Z., Liu, W., 2020. Carbon and oxygen isotopes of
742 calcified root cells, carbonate nodules and total inorganic carbon in the Chinese
743 loess-paleosol sequence: The application of paleoenvironmental studies. J. Asian
744 Earth Sci. 201,104515.
745 Ma, Y., and Feng, Q., 2015. A crucial process: organic matrix and magnesium ion
746 control of amorphous calcium carbonate crystallization on β-chitin film.
747 CrystEng Comm 17, 32.
748 Ma, Y., Zhao, J., Shao, T., Jia, Z., Zhao, Z., & Guan, Z., 2019. Hydrological cycle and
749 lake water source indicated by microrelief-evaporite-vegetation-runoff
750 assemblage of Badain Jaran Desert. Water 11(7), 1350.
751 Marasco, R., Mosqueira, María J., Fusi, M., Ramond, J. B., Merlino, G., & Booth, J.
752 M., et al., 2018. Rhizosheath microbial community assembly of sympatric desert
753 speargrasses is independent of the plant host. Microbiome, 6(1).
754 Menezes, M.N., Araújo-Júnior, H.I., Dal'Bó,P.F., Medeiros, M.A.A., 2019.
755 Integrating ichnology and paleopedology in the analysis of Albian alluvial plains
756 of the Parnaíba Basin, Brazil. Cret. Res. 96, 210-226.
757 Mercedes-Martín, R., Rogerson, M., Prior, T.J., Brasier, A.T., Reijmer, J.J.G.,
758 Billing,I.,
759 Matthews, A., Love, T., Lepley, S., Pedley, M., 2021. Towards a morphology
760 diagram for terrestrial carbonates: evaluating the impact of carbonate
761 supersaturation and alginic acid in calcite precipitate morphology, Geoch.
762 Cosmoch. Acta 306, 340-36.
763 Milliere, L., Gussone, N., Moritz, T., Bindschedler, S., Verrecchia. E.P., 2019. Origin
764 of strontium and calcium in pedogenic needle fibre calcite (NFC). Chem. Geol.
765 524, 329-344

766 Monger, H. C., Daugherty, L., Lindemann, W. C., & Liddell, C. M., 1991. Microbial
767 precipitation of pedogenic calcite. Geol. 19, 997-1000.
768 Nyachoti, S., Jin, L., Tweedie, C. E., & Ma, L., 2017. Insight into factors controlling
769 formation rates of pedogenic carbonates: a combined geochemical and isotopic
770 approach in dryland soils of the us southwest. Chem. Geol,
771 S0009254117305685.
772 ~~Pankova, E.I., Gerasimova, M.I., 2012. Properties, soil formation processes, and~~
773 ~~classification of desert soils. Arid. Ecosyst. 2 (2), 69-77.~~
774 Phillips, S.E., Milnes, A.R., and Foster, R.C., 1987, Calcified filaments: An example
775 of biological influences in the formation of calcretes in South Australia: Austr. J.
776 Soil Res. 25, 405-428.
777 Qi, J., Liu, Y., Wang, Z., Zhao, L., & Li, X., 2021. Variations in microbial functional
778 potential associated with phosphorus and sulfur cycling in biological soil crusts
779 of different ages at the Tengger desert, China. App. Soil Eco. 165, 104022.
780 Sarkar, A., and Mahapatra, S., 2012. Mechanism of unusual polymorph
781 transformations in calcium carbonate: Dissolution-recrystallization vs
782 additive-mediated nucleation. J. Chem. Sci.124(6),1399-1404.
783 Sekkal, W. & Zaoui, A.,2013. Nanoscale analysis of the morphology and surface
784 stability of calcium carbonate polymorphs. Sci. Rep. 3, 1587.
785 Simkiss, K.,1964. Variations in the crystalline form of calcium carbonate precipitated
786 from artificial sea water. Nature 201, 492-493.
787 Soil Survey Staff, 1999. Soil Taxonomy: A Basic System of Soil Classification for
788 Making and Interpreting Soil Surveys. USDA Agriculture Handbook Number
789 436. U.S. Govt. Printing Office, Washington, DC.
790 Sun, Q., Zamanian, K., Huguet, A. *et al.* 2022. Genesis and soil environmental
791 implications of intact *in-situ* rhizoliths in dunes of the Badain Jaran Desert,
792 northwestern China. Acta Geochim 41, 811–822.

Sun, Q., Wang, H., Zamanian, K., 2019a. Radiocarbon age discrepancies between the carbonate cement and the root relicts of rhizoliths from the Badain Jaran and the Tengeri deserts, Northwest China. Catena 180, 263-270.

Sun, Q., Zamanian, K., Li, Y., Wang, H., Colin, C., & Sun, H.,2019b. Carbonate crusts of Paleolake Zhuyeze, Tengeri Desert, China: Formation mechanism and paleoenvironmental implications. Quat. Int. 532,157-165.

Sun, Q. F., Xue, W.H., Zamanian, K., Colin, C., Duchampalphonse, S., Pei, W. T., 2019c. Formation and paleoenvironment of rhizoliths of Shiyang River Basin, Tengeri Desert, NW China. Quat. Int. 502, 246-257.

Sun, Q., Zamanian, K., Huguet, A. Fa, K., Wang, H., 2020. Characterization and formation of the pristine rhizoliths around *Artemisia* roots in dune soils of Tengeri Desert, NW China. Catena 193, 104633.

Sun, Q.F., Huguet, A., Zamanian, K., 2021. Outcrop distribution and formation of carbonate rhizoliths in Badain Jaran Desert, NW China. Catena 197, 104975

Golubtsov, V., Bronnikova, M., Khokhlova, O., Cherkashina, A., Turchinskaia, S., 2021. Morphological and isotopic study of pedogenic carbonate coatings from steppe and forest-steppe areas of Baikal region, South-Eastern Siberia. Catena 196, 104817.

Vepraskas, M.J., 2015. Redoximorphic Features for Identifying Aquic Conditions: North Carolina Agricultural Research Service. In: Technical Bulletin, 301.

Verrecchia, E.P., 2000. Fungi and sediments. In: Riding, R.E., Awramik, S.M. (Eds.), Microbial Sediments. Springer, Berlin, 68-75.

Verrecchia, E.P., Dumont, J.-L., Verrecchia, K.E., 1993. Role of calcium oxalate biomineralization by fungi in the formation of calcretes: a case study from Nazareth, Israel. J. Sed. Res. 63, 1000-1006.

Verrecchia, E.P., Verrecchia, K.E., 1994. Needle-fiber calcite: a critical review and a proposed classification. J. Sed. Res. A64, 650-664.

Wang, F., Sun, D., Chen, F., Bloemendal, J., Guo, F., Li, Z., Zhang, Y., Li, B., Wang, X.,2015. Formation and evolution of the Badain Jaran Desert, North China, as

revealed by a drill core from the desert centre and by geological survey. Palaeogeogr. Palaeoclimatol. Palaeoecol. 426, 139-158.

Wang, M., Dong, Z., Lu, J., Li, J., Luo, W., Cui, X., Zhang, Y., Liu, Z., Jiao, Y., Yang, L., 2015. Vegetation characteristics and species diversity around the Badain Jaran Desert. J. Desert Res. 35, 1226-1233 (In Chinese with English abstract).

Wang, N, A., Ma, N., Chen, H. B., Chen, X.L., Dong, C.Y., Zhang, Z. Y., 2013. A preliminary study of precipitation characteristics in the hinterland of Badain Jaran Desert. Adv. Water Sci. 24(2), 153-160.

Wang, X., Zhao, H., Yang, H., & Wang, K. 2019. Optical dating reveals that the height of Earth's tallest megadunes in the Badain Jaran Desert of NW China is increasing. J. Asian Earth Sci. 185, 104025.

Wang, Y., Cao, J., Zhang, X., Shen, Z., Mei, F., 2004. Carbonate content and carbon and oxygen isotopic composition of surface soil in the dust source regions of China. Mar. Geol. Quat. Geol. 24, 113-117(In Chinese with English abstract).

Wright, V.P., 1986, The role of fungal biomineralization in the formation of Early Carboniferous soil fabrics. Sediment. 33, 831-838.

Yang, X., Liu, T., & Xiao, H., 2003. Evolution of megadunes and lakes in the Badain Jaran Desert, Inner Mongolia, China during the last 31,000 years. Quat. Int. 104, 99–112

Yue, D.P., Zhao, J.B., Ma, Y.D., Huang, X.G., Shao, T.J., Luo, X.Q., Ma, A.H., 2019. Relationship between landform development and lake water recharge in the Badain Jaran Desert, China. Water 11(10), 1999.

Zeng, M., Kim, Y. Y., Anduix-Canto, C., Frontera, C., & Meldrum, F. C., 2018. Confinement generates single-crystal aragonite rods at room temperature. P.N.A. S. 115(30), 7670-7675.

Zhao, J., Chen, Z., Ma, Y., Luo, X., Chen, B., Shao, T., 2017. Film moisture with high content in sand layer and its movement in mega-dune of the Badain Jaran Desert. Sci. Geogr. Sin. 37, 960–966.

Zhao, L., Liu, Y., Yuan, S., Li, Z., & Li, X., 2020. Development of archaeal communities in biological soil crusts along a revegetation chronosequence in the Tengger desert, north central China. Soil and Till. Res. 196, 104443.

Zhang, X. C., Li, J. Y., Liu, J. L., Yuan, C. X., & Yan, X. F., 2021. Temporal shifts in cyanobacterial diversity and their relationships to different types of biological soil crust in the southeastern Tengger desert. Rhizosphere, 17, 100322.

Zhang, K., Cai, D., Ao, Y., An, Z., & Guo, Z., 2017. Local circulation maintains the coexistence of lake-dune pattern in the Badain Jaran Desert. Sci. Rep. 7, 40238.

Zhao, J., Chen, Z., Ma, Y., Luo, X., Chen, B., Shao, T., 2017. Film moisture with high content in sand layer and its movement in mega-dune of the Badain Jaran Desert. Sci. Geog. Sinica 37(6), 960-966 (in Chinese with English abstract).

Zhao, J., Shao, T., Hou, Y., 2011. Moisture content of sand layer and its origin in a mega-dune area in the Badain Jaran Desert. J. Nat. Res. 26,694-702 (in Chinese with English abstract).

Zhou, J., Chafetz, H.S., 2009. Biogenic caliches in Texas: the role of organisms and effect of climate. Sediment. Geol. 222, 207-225.

Zhu, J., Wang, N., Chen, H., Dong, C., & Zhang, H., 2010. Study on the boundary and the area of Badain Jaran Desert based on the remote sensing imagery. Prog. Geogr. 29, 1087-1094 (in Chinese with English abstract).

Zhu, R., Li, Z., Gao, Y., Chen, Q., & Yu, Q., 2019. Variations in chemical element compositions in different types of Holocene calcareous root tubes in the Tengger Desert, NW China, and their palaeoenvironmental significance. Boreas 48(3), 800-809.

Zhu, T., & Maria, D., 2016. Carbonate precipitation through microbial activities in natural environment, and their potential in biotechnology: A review. Fron. Bioeng. Biotechn. 4, 4.

Figures and Captions

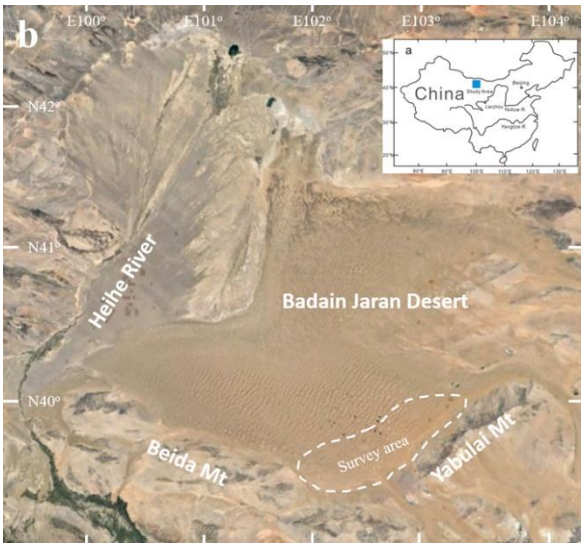

Fig.1. Location (blue square) of the BJD in China (a) and the exploration area (white dash lines) in the desert (b, Revised from https://earth.google.com).

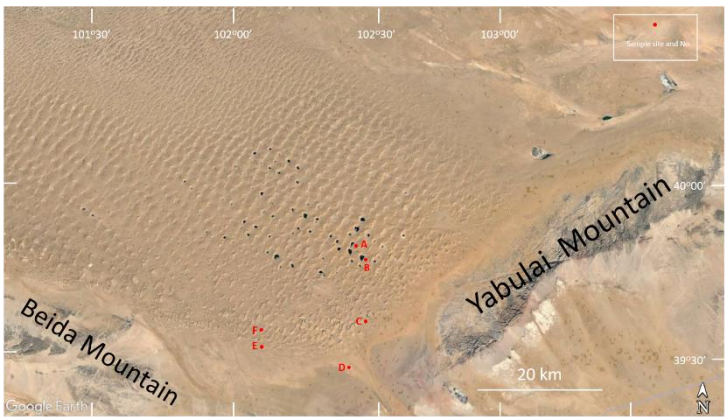

Fig.2. Detail of the sampling sites (A-F) in the southeastern desert. (A-Sumujilin Lake, B-Nuoertu Lake, C-Baoritaolegai Lake, D-The Gate of National Geological Park of BJD, E & F-random sites among the dunes. Revised from https://earth.google.com)

Fig. 3. a-Fragments of caliche and rhizoliths (The spade length is 100 cm). b-Hard varnished rhizoliths (The diameter of the coin is 20 mm).

Fig. 4. White pieces of rhizoliths and a root tube. Relicts of fine root hairs within the tube and weathered rills are observed on the surface of the tube.

Fig. 5. a-Vertical PRs dug out of soil (the red screwdriver handle length is 10 cm). b-Root relicts with central cavity and beige peripheral part of PRs in Fig a.

Fig. 6. Brown interior of the PR with root relicts.

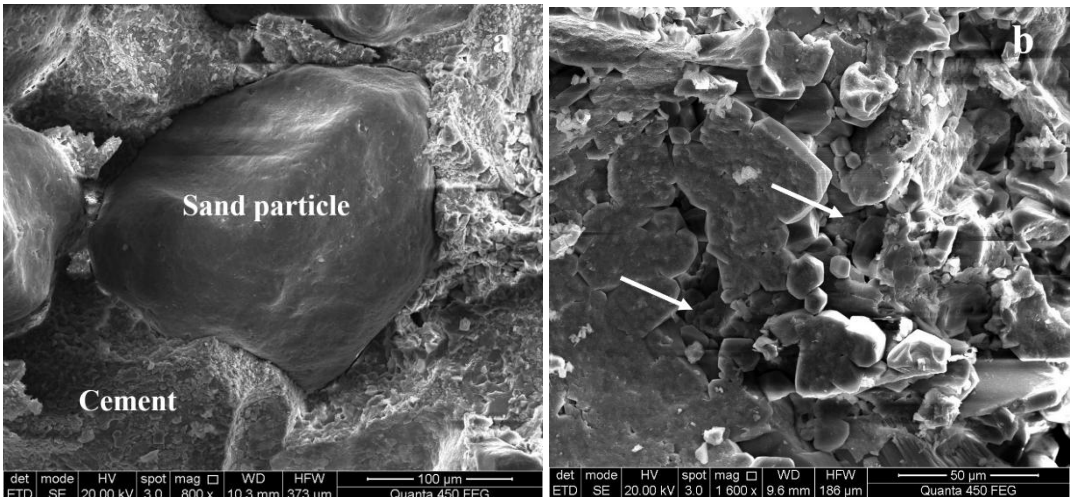

916

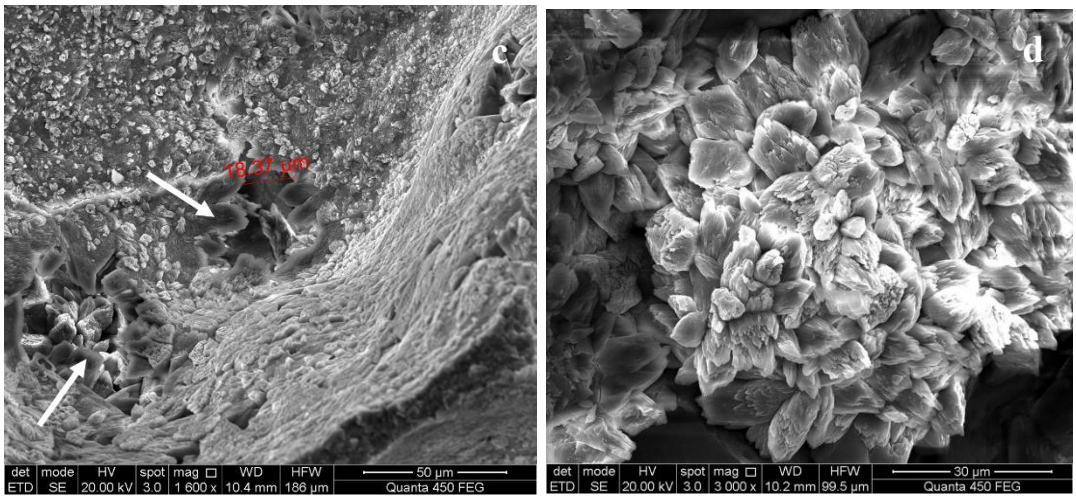

917

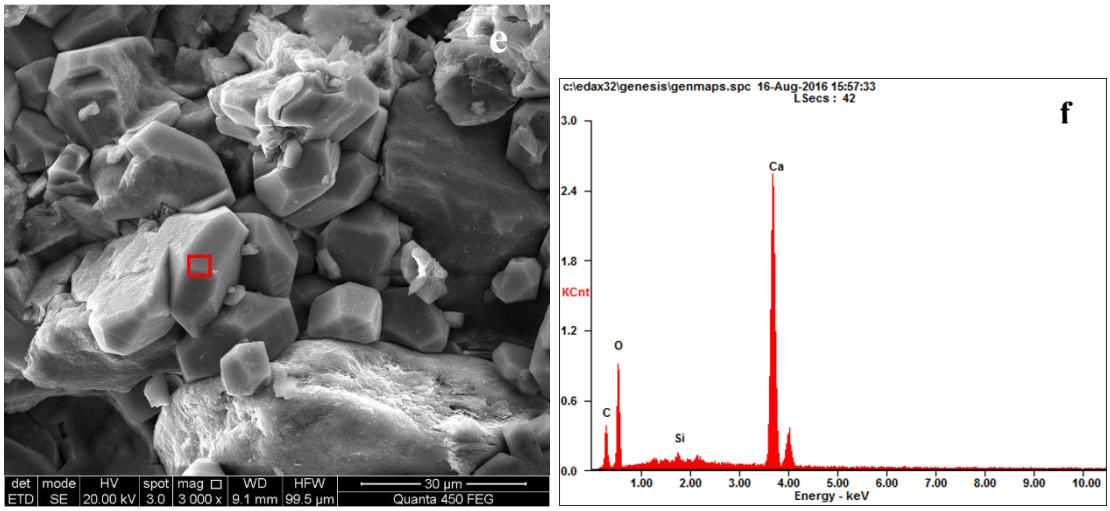

918 Fig.7. a-SEM microstructures of RRs. b-Polyhedral crystal cement and pores (white arrows). c-Some
919 of the cementing crystals are bigger euhedral rhombic crystals, showing prismatic/tooth-like shape
920 around the walls of the pores (white arrows). d-Aragonite rosette by morphology. e-Cement
921 polyhedral crystals, showing well-developed equant faces and slightly smooth edges and corners. The
922 crystals are modified scalenohedral or pentagonal repeated twins. The red square is the focus of the of
923 EDS analysis (same for the following Figs. 8-12). f-EDS spectrum reveals that the cement is made of
924 calcite (of Fig. e).

925

926

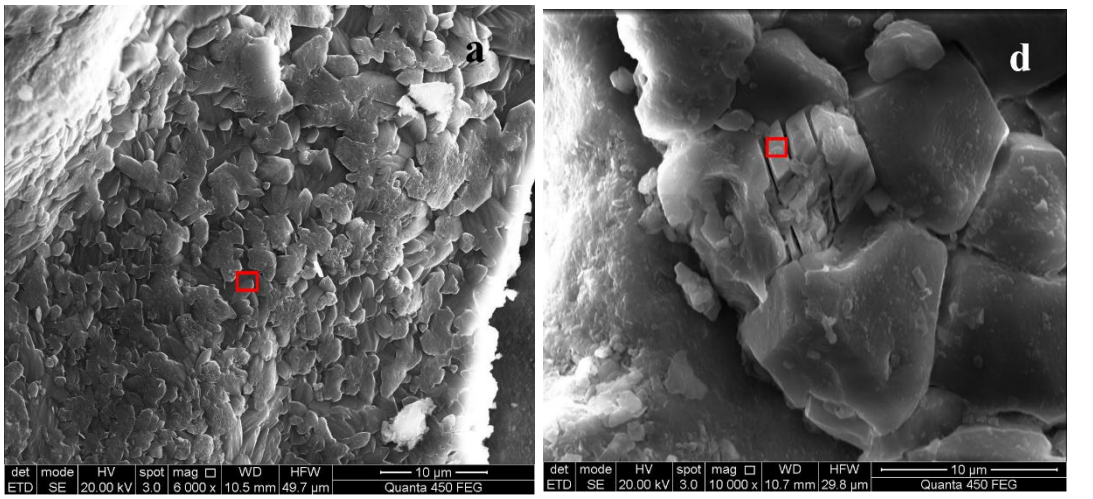

927

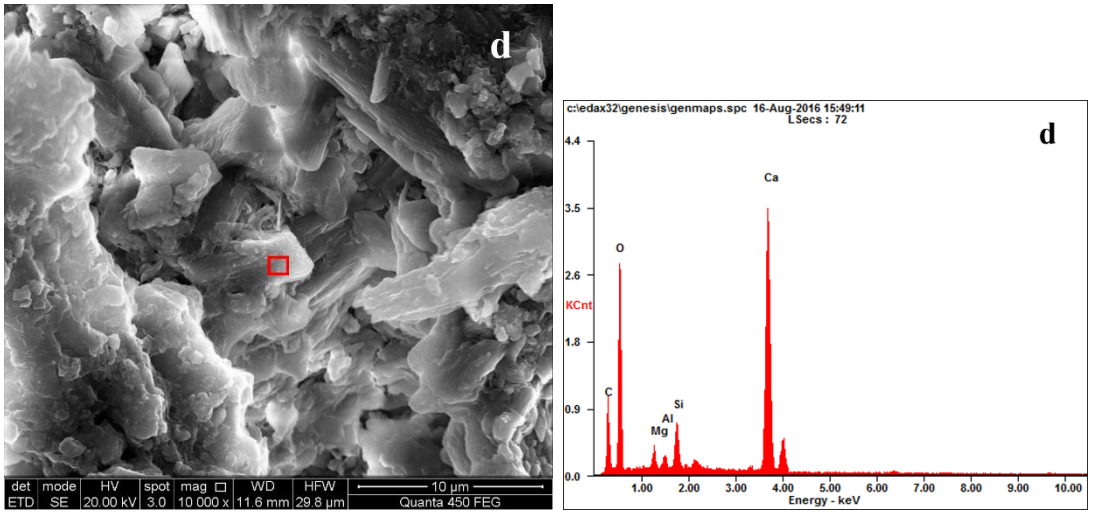

928 Fig.8. a-Spherular cementing minerals. b-Monocrystalline polyhedral calcites of cement. The EDS
929 results of Fig. a and b were omitted. c-Short rods. d-EDS spectrum (of Fig. c) reveals cement
930 calcium carbonate with a little portion of Mg.

931

932

933 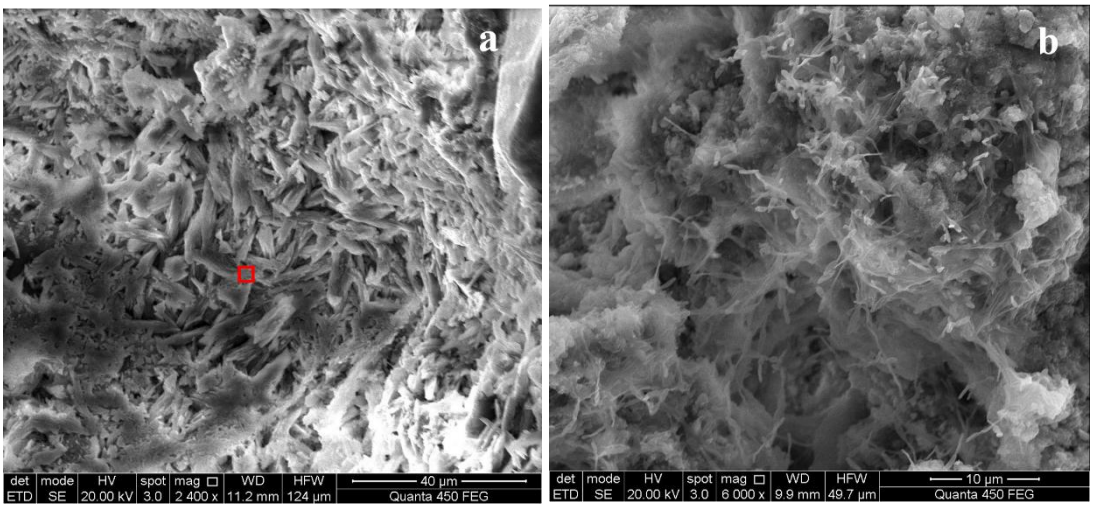

934 Fig.9. a-Short rods of aragonite. b-Hair-like, or fungi-form crystals of cement with pores, cavities

935 and voids.

936

937 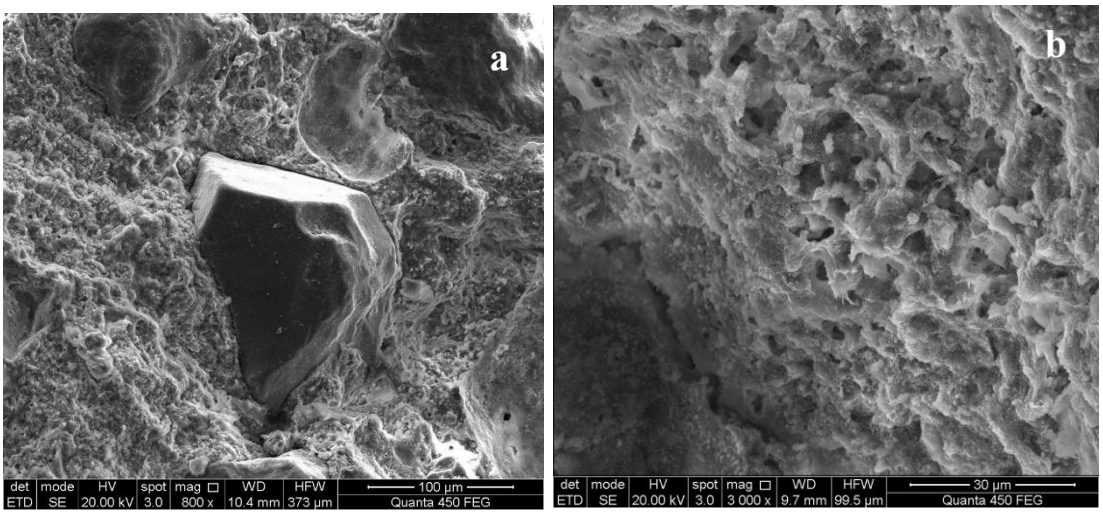

938 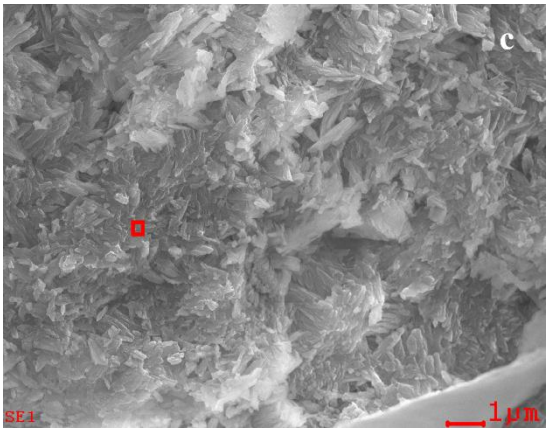

Fig.10. a-Calcite cement around a sand particle, showing homogeneous micritic mass (PR). b-Pores, cavities and voids among the micritic mass (PR). c-Dense cement of prism/pillar-like calcite (PR).

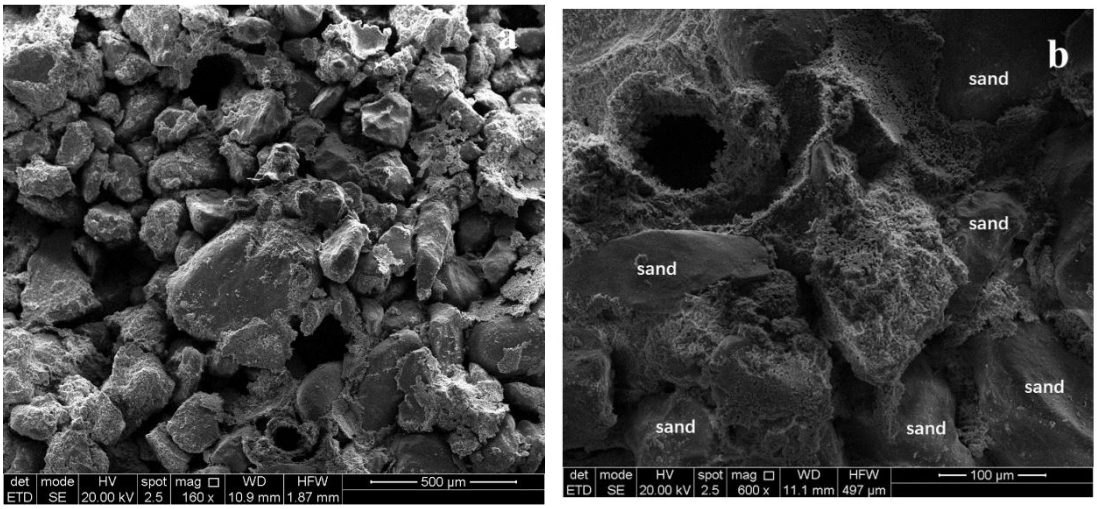

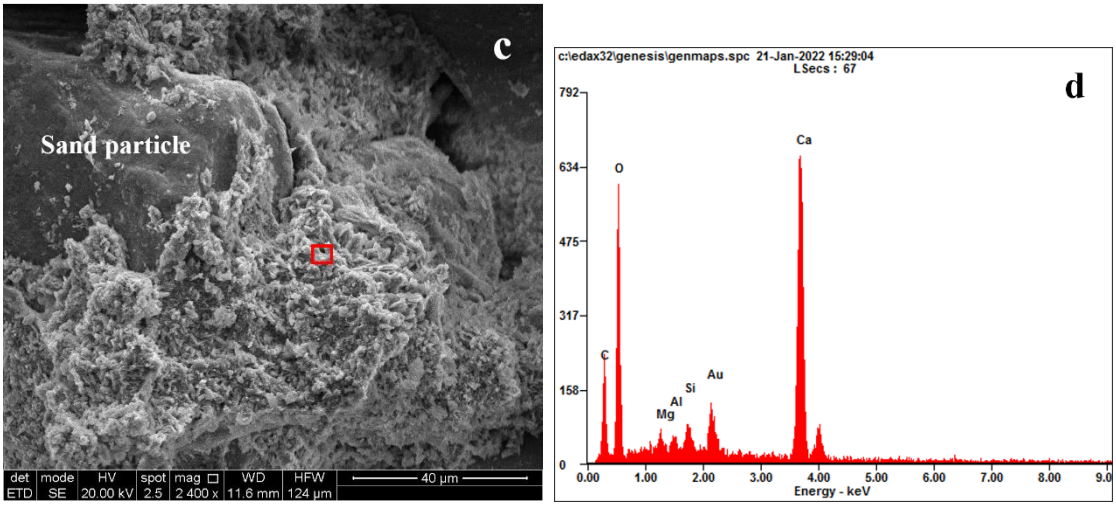

Fig. 11. a-The cementing minerals are mostly as coatings on sand particles and the cement cannot fill and plug the pores among sand particles. Therefore, large pore spaces among the particles remain empty and the particles are loose because of a porous cement. b-The cementing minerals are homogeneous micritic mass. c-The homogeneous micritic mass is forming thin layers on the surfaces of particles. d-EDS spectrum (of c) reveals that the cement is mainly constituted of calcium carbonate with only a little Mg.

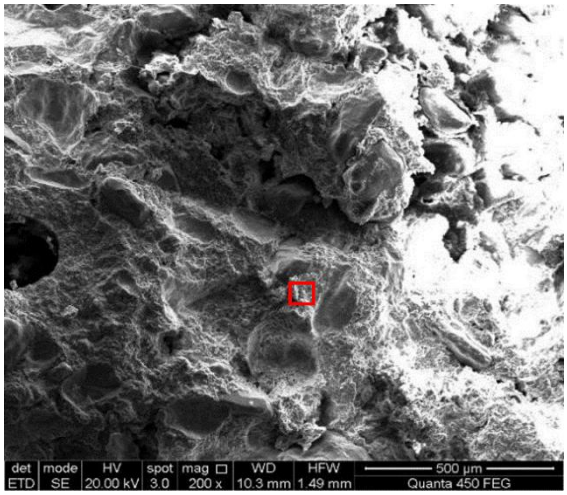

Fig. 12. Homogeneous micritic mass.

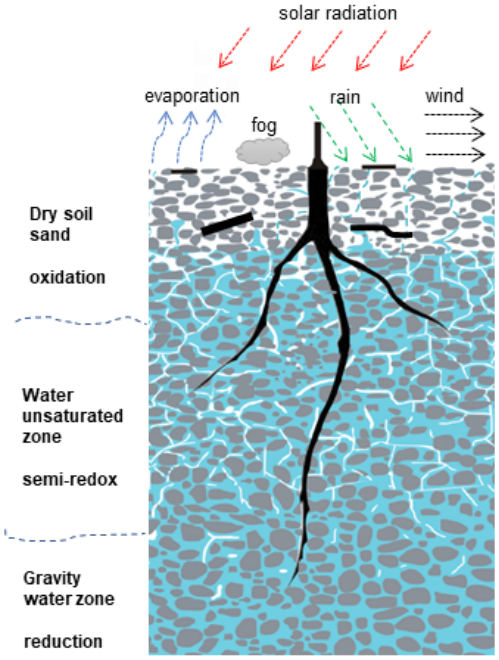

Rhizolith type	Diagenesis environment	Site and cement crystal morphology						
		A	B	C	D	E	F	Key features
reworked	strong wind, solar radiation, dry soil (~30 cm depth), open soil, changing temperatures	polyhedral, euhedral rhombic. rosette. calcium carbonate	Polyhedral. short rods. Mg calcium carbonate	short rods . hair-like, or fungi-form crystals calcium carbonate	short rods	(upper RR was not analysed)	short rods	clear crystal shapes, short rods
primary	wet soil, semi-closed/closed condition, stable temperatures, soil water unsaturated zone (~200 cm depth)				homogeneous micritic mass. pillar-like calcite. with pores, cavities and voids Mg calcium carbonate	homogeneous micritic mass calcium carbonate	homogeneous micritic mass, with pores, cavities and voids calcium carbonate	homogeneous micritic mass, with pores, cavities and voids

Fig. 13. Rhizolith types, diagenesis environment, micro-morphologies and compositions of cementing minerals at different sites.

964

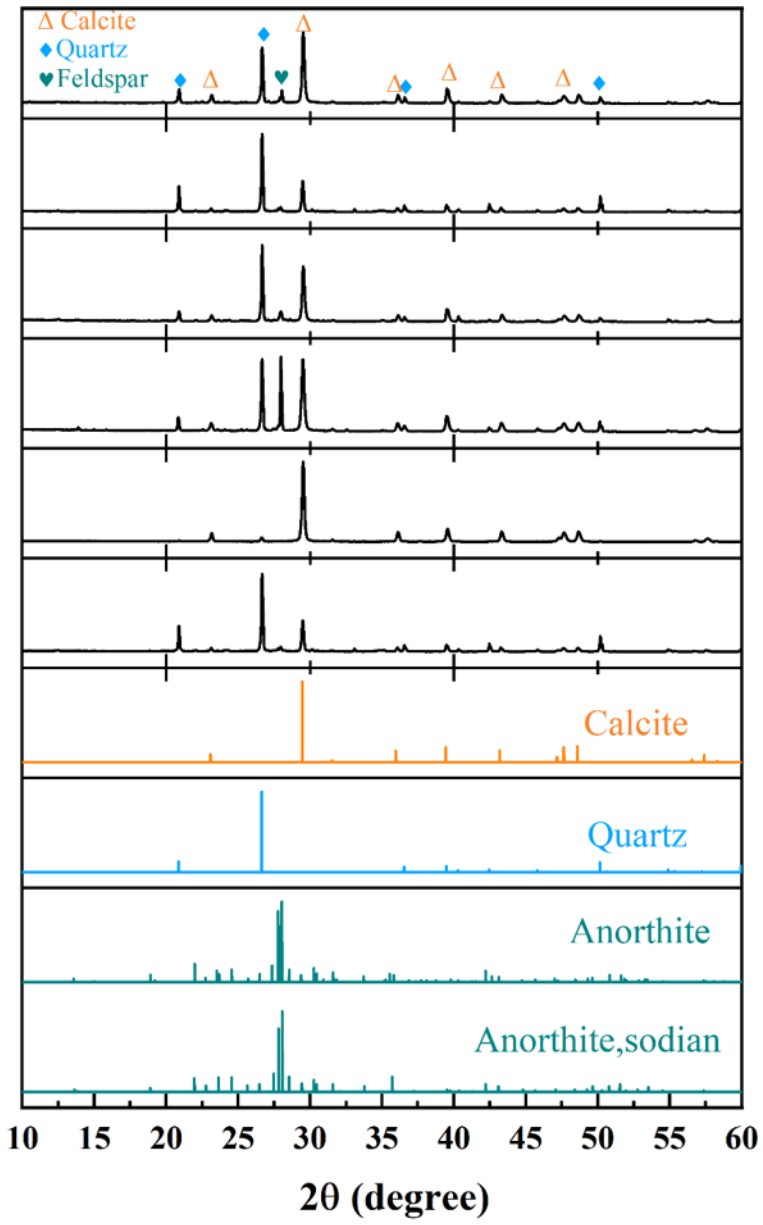

965

966 Fig. 14. XRD patterns of the cements collected at different sites: a-Site A, b-Site B, c-Site C, d-Site D,

967 e-Site E, f-Site F. The standard card numbers of calcite, quartz, and anorthite used here are #86-2334,

968 #85-0797 and #10-0393, respectively.

969